# Leveraging Blur Information with a Multi-Focus Plenoptic Camera: Calibration, Relative Blur calibration and characterization

**Mathieu Labussière**[1] Céline Teulière[1] Frédéric Bernardin[2] Omar Ait-Aider[1]

12 Nov. 2020

Journée thématique GdR ISIS - Capteurs visuels émergents : vision plénoptique

[1]Université Clermont-Auvergne, CNRS, SIGMA Clermont, Institut Pascal, F-63000 Clermont-Ferrand, France
[2]Cerema, Équipe-projet STI, 10 rue Bernard Palissy, F-63017 Clermont-Ferrand, France

**Contact**: mathieu.labu@gmail.com, firstname.name@{uca,cerema}.fr

# Table of contents

# Background

# Imaging System

Pixel collects radiance from light rays. Radiance can be modeled by the plenoptic function[1]

$$\mathcal{L}\left(\boldsymbol{x}, \boldsymbol{\theta}, \lambda, \tau\right) \tag{1}$$

where:

- $\boldsymbol{x} \in \mathbb{R}^3$ is the spatial position of observation in space,
- $\boldsymbol{\theta} \in \mathbb{R}^2$ is the angular direction of observation in space,
- $\lambda \in \mathbb{R}$ is the wavelength of light and $\tau \in \mathbb{R}$ is the time.

| Sensors | Spatial ($\boldsymbol{x}$) | Angular ($\boldsymbol{\theta}$) |
|---|---|---|
| classic camera | ✓ | - |
| plenoptic camera | ✓ | ✓ |

[1] Adelson et al., 1991.

# How to acquire the plenoptic function?

From Lippmann's Lumigraph to commercial plenoptic cameras[2], several designs have been proposed to capture spatial as well as angular information.

**Figure 1:** The `Lytro Illum` camera

**Figure 2:** The `Raytrix R12` camera

[2] Ng et al., 2005; Perwaß et al., 2012.

# With the (Multi-Focus) Plenoptic Camera

Plenoptic cameras based on a Micro-Lenses Array (MLA) placed between the main lens and the photo-sensible sensor

The MLA has different lens types with different focal lengths

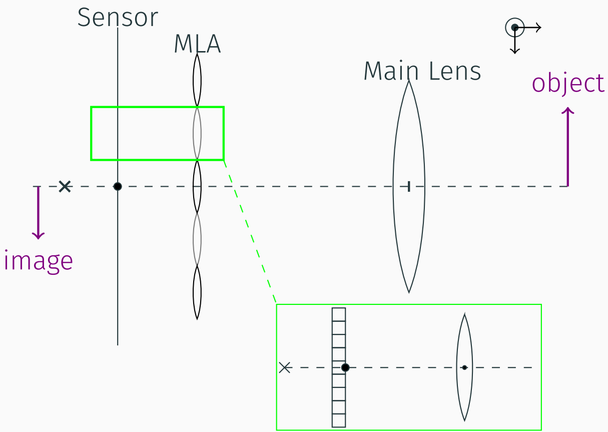

# With the (Multi-Focus) Plenoptic Camera

Multiplexing both angular and spatial information onto the sensor in the form of a Micro-Images Array (MIA)

---

Trade-off between the angular and spatial resolution

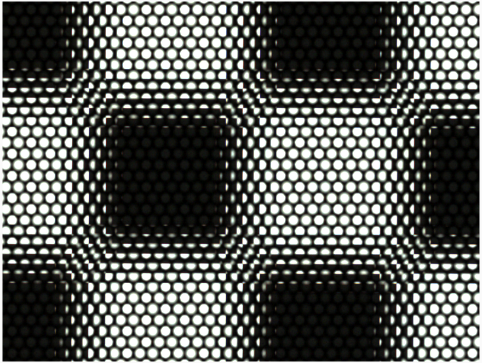

Main lens = thin-lens + lateral distortion (radial and tangential)

Two configurations : Galilean (projection behind the MLA) and Keplerian (in front of the MLA)

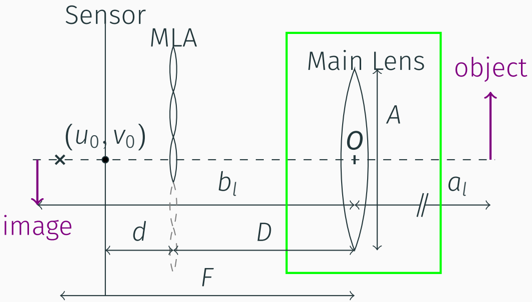


Thin-lens equation:

$$\frac{1}{F} = \frac{1}{a_l} + \frac{1}{b_l} \tag{2}$$

# The Plenoptic Camera Model - Micro-Lenses Array (MLA)

Micro-lenses = thin-lenses + 6-dof pose + optical centers

---

Take into account blur in the micro-image

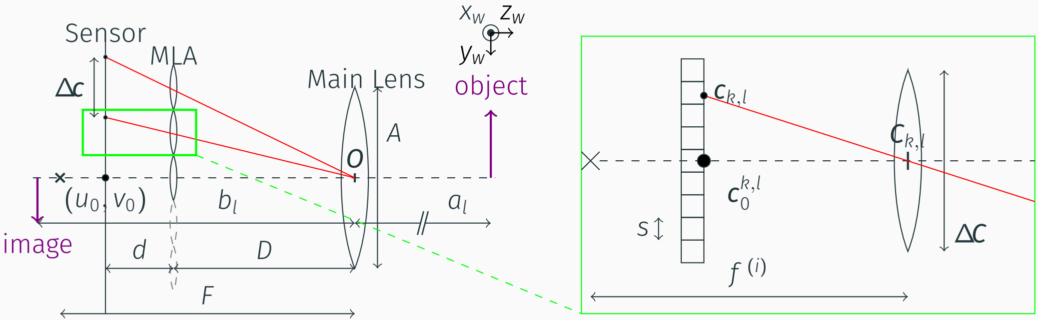

# Problematic

Multi-focus configuration $\longrightarrow$ same part of a scene will be more or less focused w.r.t. the micro-lens type

Usually, only micro-images with the smallest amount of blur are used:

$$\text{Blur} \longrightarrow \text{drawback}$$

To exploit all the information available, we propose to explicitly model the defocus blur in a new camera model:

$$\text{Blur} \longrightarrow \text{information}$$

# Blur Aware Calibration of Multi-Focus Plenoptic Camera

# Our contributions

Our calibration method[3] is the first:

- proposing a single optimization process that retrieves intrinsic and extrinsic parameters,
- including a more complete model of the multi-focus plenoptic camera,
- working directly from raw images.

---

This is achieved by introducing a new Blur Aware Plenoptic (BAP) feature defined in raw image space that enables us to handle the multi-focus case.

[3] Mathieu Labussière et al. (2020). "Blur Aware Calibration of Multi-Focus Plenoptic Camera". In: *Proceedings of the IEEE/CVF Conference on Computer Vision and Pattern Recognition (CVPR)*, pp. 2545–2554.

# Leveraging blur information with our Blur Aware Plenoptic (BAP) Feature

Blurred image of a point = blur circle

Our new Blur Aware Plenoptic (BAP) feature is characterized by its center and its radius:

$$p = (u, v, \rho)\,. \tag{3}$$

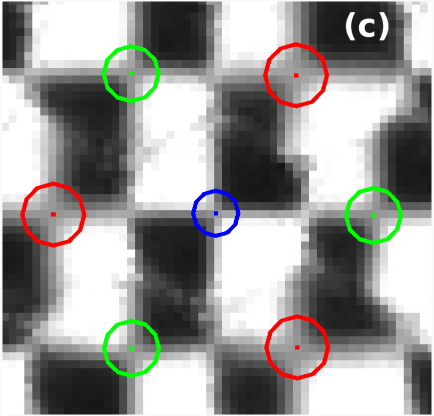

# Projecting scene point through our camera model

Linking a scene point $\boldsymbol{p}_w$ to our new BAP feature $\boldsymbol{p}$ through each micro-lens $(k, l)$

$$\begin{bmatrix} u \\ v \\ \rho \\ 1 \end{bmatrix} \propto \mathcal{P}(i, k, l) \cdot T_{\mu}(k, l) \cdot \varphi(K(F) \cdot T_c \cdot \boldsymbol{p}_w) \,. \tag{4}$$

where:

- $\mathcal{P}(i, k, l)$ = blur aware plenoptic projection matrix
- $K(F)$ = thin-lens projection matrix
- $T_c$ = main lens' pose
- $T_{\mu}(k, l)$ = micro-lens' pose
- $\varphi(\cdot)$ = lateral distortions.

# Pre-calibration using raw white images for internal parameters estimation

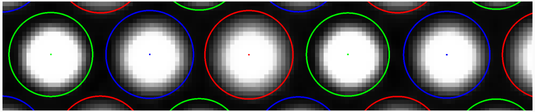

$N = 5.657$

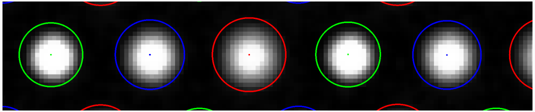

$N = 8$

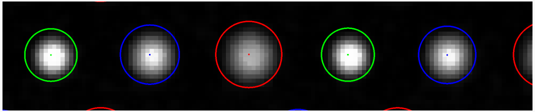

$N = 11.31$

From raw white images, the micro-image (MI) radius $R$ is expressed as a linear function of the inverse $f$-number $N^{-1}$:

$$\mathrm{R_i}\left(N^{-1}\right) = m \cdot N^{-1} + q_i. \qquad (5)$$

The internal parameters $\Omega = \{m, q_1, \ldots, q_i\}$ are estimated for each micro-lens of type $i$ from radii measurements.

# Detecting BAP feature through micro-lenses in raw images

1. Corners are detected at position $(u, v)$ using the detector of Noury et al. (2017)[4],
2. Radii $\rho$ through micro-lenses $i$ are computed directly in raw image space by:

$$\rho = \frac{\Delta c}{2 \cdot s} \cdot \nu^{-1} + \frac{1}{s} \cdot \left( q_i - \frac{\Delta c}{2} \right) \tag{6}$$

where

- $s$ = pixel size,
- $\Delta c$ = distance between two micro-images center,
- $\nu$ = virtual depth = relative depth value from disparity.

[4] Charles Antoine Noury et al. (2017). "Light-Field Camera Calibration from Raw Images". In: *DICTA 2017 – International Conference on Digital Image Computing: Techniques and Applications*, pp. 1–8.

# Retrieving camera parameters with our non-linear optimization

Introducing the blur aware plenoptic reprojection error to be minimized by our non-linear optimization process of our single calibration.

Let $\mathcal{S} = \{\Xi, \{T_c^n\}\}$ be the set of intrinsic $\Xi$ and extrinsic $\{T_c^n\}$ parameters to be optimized.

$$\Theta(\mathcal{S}) = \underbrace{\sum \left\| p_{k,l}^n - \pi_{k,l}\left(p_w^n\right) \right\|^2}_{\text{blur aware plenoptic reprojection error}} + \underbrace{\sum \left\| c_{k,l} - \pi_{k,l}\left(O\right) \right\|^2}_{\text{micro-lens center reprojection error}} . \tag{7}$$

Optimization $\longrightarrow$ Levenberg-Marquardt algorithm

# Our experimental setup

`Raytrix R12`, multi-focus plenoptic camera with:

- a mounted lens of 50mm focal length,
- a MLA composed of 3 micro-lens types,
- a pixel size of $s = 5.5\mu m$.


Building 3 datasets for 3 focus distances $h$:

- R12-A for $h = 450$ mm,
- R12-B for $h = 1000$ mm,
- R12-C for $h = \infty$.

# Qualitative reprojection error experiment

Qualitative evaluation $\longrightarrow$ reprojection error using the previously computed intrinsics

Metric $\longrightarrow$ Root-Mean-Square Error (RMSE) in pixel.

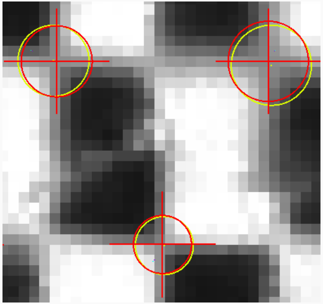

| | R12-A (#11424) | | R12-B (#3200) | | R12-C (#9568) | |
|---|---|---|---|---|---|---|
| | Total | RMSE | Total | RMSE | Total | RMSE |
| $\bar{\epsilon}_{all}$ | 8972.91 | 0.886 | 1444.98 | 0.672 | 5065.33 | 0.728 |
| $\bar{\epsilon}_{u,v}$ | 8908.65 | 0.883 | 1345.20 | 0.648 | 5046.68 | 0.726 |
| $\bar{\epsilon}_{\rho}$ | 64.257 | 0.075 | 99.780 | 0.177 | 18.659 | 0.044 |

**Table 1:** Reprojection error (with their number of observations), and the total squared pixel error with its RMSE.

# Quantitative evaluation in a controlled environment

Quantitative evaluation $\longrightarrow$ poses estimation with the previously computed intrinsics on linear motion table with micro-metric precision

Metric $\longrightarrow$ relative translation error w.r.t. known relative motion (ground truth)

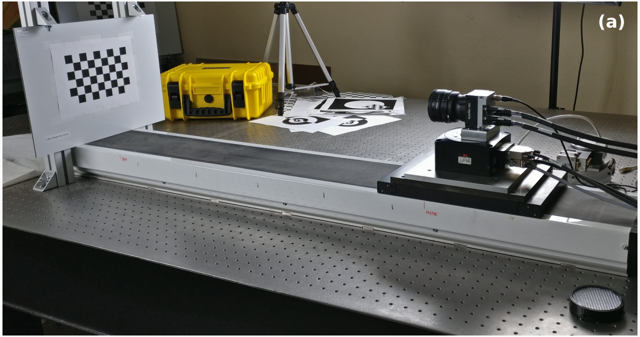

# Quantitative evaluation in a controlled environment

For our method:

- stable behavior across all datasets,
- the lowest mean error on all datasets.

| | R12-A | | R12-B | | R12-C | | All |
|---|---|---|---|---|---|---|---|
| Error [%] | $\bar{\epsilon}_z$ | $\sigma_z$ | $\bar{\epsilon}_z$ | $\sigma_z$ | $\bar{\epsilon}_z$ | $\sigma_z$ | $\bar{\epsilon}_z$ |
| Ours | 3.73 | 1.48 | 3.32 | 1.17 | 2.95 | 1.35 | **3.33** |
| Noury et al. (2017) | 6.83 | 1.17 | 1.16 | 1.06 | 2.70 | 0.86 | 3.56 |
| `RxLive` (v.4.0) | 4.63 | 2.51 | 4.26 | 5.79 | 11.52 | 3.22 | 6.80 |

**Table 2:** Relative translation error along the $z$-axis with respect to the ground truth displacement. The mean error $\bar{\epsilon}_z$ and its standard deviation $\sigma_z$ are given for our method, Noury et al. (2017) method, and for the proprietary software `RxLive`.

# Concluding remarks on calibration

We introduced a new Blur Aware Plenoptic (BAP) feature:

- defined in raw image space that enables us to handle the multi-focus case,
- exploited in our single calibration process,
- to retrieve parameters of a more complete camera model.

Validated by qualitative experiments and quantitative evaluations.

# Code sources and datasets redistribution

LibPlen

- The libpleno, an open-source C++ library for plenoptic camera:
  → https://github.com/comsee-research/libpleno
- Compote, a set of tools to pre-calibrate and calibrate a multi-focus plenoptic camera:
  → https://github.com/comsee-research/compote
- Our datasets R12-ABC:
  → https://github.com/comsee-research/plenoptic-datasets

# Relative Blur Calibration

# Analyzing the Relative Blur between micro-image - PSF

Point-Spread Function = the response of an imaging system to an unresolved object = blur.

---

Blurred image, $\mathcal{I}(x, y)$, of object at a constant distance = convolution of the PSF, $\mathrm{h}(x, y)$, with the focused image, $\mathcal{I}^*(x, y)$, such as:

$$\mathcal{I}(x, y) = \mathrm{h} * \mathcal{I}^*(x, y)\,. \tag{8}$$

# Analyzing the Relative Blur between micro-image - PSF

Point-Spread Function (PSF) $\mathrm{h}(x, y)$ of a circular lens $\longrightarrow$ 2-dimensional Gaussian,

$$\mathrm{h}(x, y) = \frac{1}{2\pi\sigma^2} \exp\left(-\frac{x^2 + y^2}{2\sigma^2}\right), \tag{9}$$

where $\sigma$ = the spread parameter, proportional to the blur circle radius $\rho$, i.e.,

$$\sigma \propto \rho \Leftrightarrow \sigma = \kappa \cdot \rho \tag{10}$$

where $\kappa$ = camera constant that should be determined by calibration[5].

The spatially-variant spread parameter is depending of the object distance $a$.

[5] Pentland, 1987; Subbarao, 1989.

# Analyzing the Relative Blur between micro-image

For 2 different micro-lens types $(i)$ and $(j)$ $\longrightarrow$ different blur level = different spread parameter for the PSF model:

$$\begin{cases} \mathcal{I}_{(i)}(x,y) = \mathrm{h}_{(i)} * \mathcal{I}^*(x,y) \\ \mathcal{I}_{(j)}(x,y) = \mathrm{h}_{(j)} * \mathcal{I}^*(x,y) \end{cases} \tag{11}$$

with $\sigma_{(i)}$ the diameter of the blur kernel $\mathrm{h}_{(i)}$.

The equally-defocused representation is then

$$\begin{cases} \mathcal{I}_{(i)}(x,y) \simeq \mathrm{h}_r * \mathcal{I}_{(j)}(x,y) & \text{if } \sigma_{(i)} \leq \sigma_{(j)} \\ \mathrm{h}_r * \mathcal{I}_{(i)}(x,y) \simeq \mathcal{I}_{(j)}(x,y) & \text{if } \sigma_{(i)} \geq \sigma_{(j)} \end{cases} \tag{12}$$

# Analyzing the Relative Blur between micro-image

The diameter of the relative blur kernel $\mathbf{h}_r$ is approximated as

$$\sigma_r(i,j) \simeq \sqrt{|\sigma^2_{(i)} - \sigma^2_{(j)}|}. \tag{13}$$

---

We defined then the relative blur as

$$\Delta\sigma^2(i,j) = \sigma^2_{(j)} - \sigma^2_{(i)} \text{ with } \begin{cases} \Delta\sigma^2(i,j) > 0 & \text{if } (i)\text{-view is more in-focus} \\ \Delta\sigma^2(i,j) \leq 0 & \text{if } (j)\text{-view is more in-focus} \end{cases} \tag{14}$$

---

Analogously the relative blur radius is given by

$$\rho_r(i,j) \simeq \sqrt{|\Delta\rho^2(i,j)|} = \sqrt{|\rho^2_{(j)} - \rho^2_{(i)}|} \text{ with } \sigma_r = \kappa \cdot \rho_r. \tag{15}$$

# Relative Blur calibration using BAP features

BAP features $\{\boldsymbol{p}_i\}$ from a same cluster $\mathcal{C}$ represent the same point in object space $\boldsymbol{p}_w$.

Two windows $\mathcal{W}$ extracted around two BAP features $\boldsymbol{p}_i, \boldsymbol{p}_j \in \mathcal{C}(\boldsymbol{p}_w)$ of different types, can be expressed using the equally-defocused representation.

- here, additional blur is done applying a Gaussian kernel of spread parameter $\sigma_r$
- the spread parameter is computed using the $\rho$ part of the BAP features and the parameter $\kappa$ to be optimized (initial value $\check{\kappa} = 1$)
- windows $\mathcal{W}$ of size $9 \times 9$ are extracted at $(u, v)$ with sub-pixel precision

# Relative Blur calibration using BAP features

Let $\kappa$ be the parameter to be optimized, and $\Theta(\kappa)$ the objective function to be minimized:

$$\Theta(\kappa) = \sum_{n} \sum_{\boldsymbol{p}_i^n, \boldsymbol{p}_j^n \in \mathcal{C}(\boldsymbol{p}_w^n)} \left\| \mathcal{W}\left(\boldsymbol{p}_j^n\right) - \mathrm{h}_r * \mathcal{W}(\boldsymbol{p}_i^n) \right\|_{\ell_1} \text{ given } \rho_{(i)} < \rho_{(j)}, \tag{16}$$

where $\sigma_r = \kappa \cdot \sqrt{|\rho_{(j)}^2 - \rho_{(i)}^2|}$.

Optimization $\longrightarrow$ Levenberg-Marquardt algorithm

Using the R12-ABC datasets, we obtain $\hat{\kappa} = 0.680851$.

# Concluding remarks on relative blur calibration

Using our Blur Aware Plenoptic (BAP) feature we are now able to link the geometric blur (i.e., the circle of confusion) to the physical blur (i.e., the point spread function).

- fully exploit blur in image space with physical meaning $\longrightarrow$ rendering, de-convolution, etc.
- the amount of blur is link to depth $\longrightarrow$ depth estimation

# Characterization of the Plenoptic Camera

# Characterizing the Plenoptic Camera

Camera characterization from camera model parameters (obtained by calibration):

- Minimal acceptable circle of confusion ($r_0 = s/2$)
- Near-focus ($a_-$), Far-focus ($a_+$) et Focus planes ($a_0^{(i)}$)
- Total depth of field ($\mathrm{DOF} = \max_i\{|{a_+}^{(i)}|\} - \min_i\{|{a_-}^{(i)}|\}$)
- Blur profile, i.e., blur radius as function of the distance

Analysis in MLA space $\longrightarrow$ object space by projection

# Characterizing the Plenoptic Camera - Blur radius

The blur radius $\rho$ of a point at a distance $a$ through a lens of aperture $A$ and with a focal length $f$ onto a sensor at a distance $d$:

$$\begin{cases} r = A\dfrac{d}{2}\left(\dfrac{1}{f} - \dfrac{1}{a} - \dfrac{1}{d}\right) & \text{[metric]} \\ \rho = \dfrac{r}{s} & \text{[pixelic]} \end{cases} \tag{17}$$

The minimal acceptable radius of the circle of confusion (CoC) is computed as half the size of a pixel, such as $r_0 = s/2$.

# Characterizing the Plenoptic Camera - Focus Planes

In MLA space, for a a micro-lens of type $(i)$, the focus plane distance is given by:

$$a_0^{(i)} = \left( \frac{1}{f^{(i)}} - \frac{1}{d} \right)^{-1} = \frac{d f^{(i)}}{d - f^{(i)}}. \tag{18}$$

We derived the far $a_+$ and near $a_-$ focus planes distances, such as:

$$a_+ = \frac{dA \cdot a_0}{fA - 2r_0 \left( a_0 - f \right)} \quad \text{[far]} \tag{19}$$

and

$$a_- = \frac{dA \cdot a_0}{fA + 2r_0 \left( a_0 - f \right)} \quad \text{[near].} \tag{20}$$

# Characterizing the Plenoptic Camera - Depth of Field

The depth of field (DoF) of a micro-lens of type $(i)$ is computed as the distance between the near and far focus planes, such as

$$\mathrm{DOF}^{(i)} = |a_+| - |a_-| = \frac{fA \cdot a_0 \cdot 2r_0\,(a_0 - f)}{(fA)^2 - 4{r_0}^2\,(a_0 - f)^2}. \tag{21}$$

Finally, the total DoF of the plenoptic camera in MLA space is computed using the micro-lenses DoFs as

$$\mathrm{DOF} = \max_i\{|{a_+}^{(i)}|\} - \min_i\{|{a_-}^{(i)}|\}. \tag{22}$$

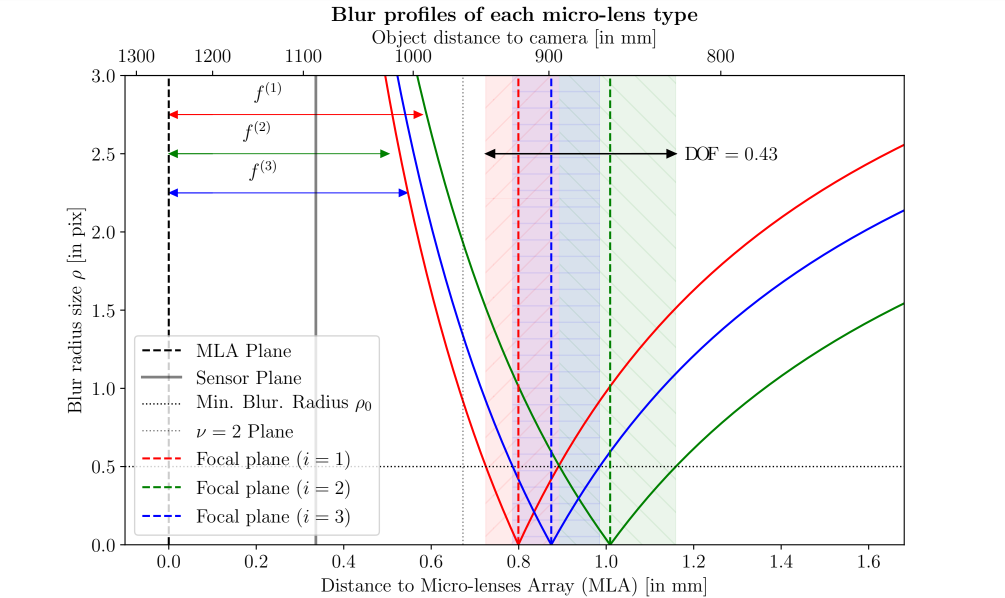
Blur profiles of each micro-lens type
Object distance to camera [in mm]
1300
1200
1100
1000
900
800
$f^{(1)}$
$f^{(2)}$
$f^{(3)}$
DOF = 0.43
Blur radius size $\rho$ [in pix]
3.0
2.5
2.0
1.5
1.0
0.5
0.0
MLA Plane
Sensor Plane
Min. Blur. Radius $\rho_0$
$\nu = 2$ Plane
Focal plane ($i = 1$)
Focal plane ($i = 2$)
Focal plane ($i = 3$)
0.0
0.2
0.4
0.6
0.8
1.0
1.2
1.4
1.6
Distance to Micro-lenses Array (MLA) [in mm]

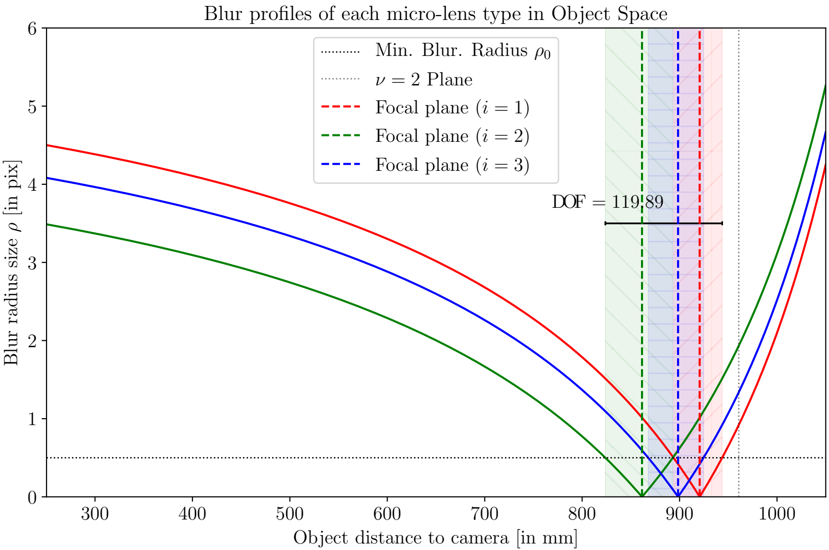
Blur profiles of each micro-lens type in Object Space
Min. Blur. Radius $\rho_0$
$\nu = 2$ Plane
Focal plane ($i = 1$)
Focal plane ($i = 2$)
Focal plane ($i = 3$)
DOF = 119.89
Blur radius size $\rho$ [in pix]
Object distance to camera [in mm]
0
1
2
3
4
5
6
300
400
500
600
700
800
900
1000

# Conclusion

# Conclusion

By leveraging blur information we are able to:

- propose a more complete camera model by introducing a new BAP feature that explicitly model the defocus blur,
- fill the gap between the physical blur and geometric blur to open a whole set of new applications leveraging blur, like for instance depth estimation,
- and, characterize the plenoptic camera to fully exploit its extended depth of field (DoF).

# Acknowledgments

This work has been sponsored by the AURA Region and the European Union (FEDER) through the MMII project of CPER 2015-2020 MMaSyF challenge.

We thank Charles-Antoine Noury and Adrien Coly for their insightful discussions and their help during the acquisitions.

# References


- Adelson, E. H. and J. R. Bergen (1991). "The plenoptic function and the elements of early vision". In: *Computational Models of Visual Processing*, pp. 3–20.
- Bok, Yunsu, Hae-Gon Jeon, and In So Kweon (2014). "Geometric Calibration of Micro-Lens-Based Light-Field Cameras Using Line Features". In: *Computer Vision – ECCV 2014*. Springer International Publishing, pp. 47–61.
- – (2017). "Geometric Calibration of Micro-Lens-Based Light Field Cameras Using Line Features". In: *IEEE Transactions on Pattern Analysis and Machine Intelligence* 39.2, pp. 287–300.

# References ii


- Dansereau, Donald G., Oscar Pizarro, and Stefan B. Williams (2013). "Decoding, calibration and rectification for lenselet-based plenoptic cameras". In: *Proceedings of the IEEE Computer Society Conference on Computer Vision and Pattern Recognition*, pp. 1027–1034.
- Hahne, Christopher et al. (2018). "Real-time refocusing using an FPGA-Based standard plenoptic camera". In: *IEEE Transactions on Industrial Electronics* 65.12, pp. 9757–9766.
- Heinze, Christian et al. (2016). "Automated Robust Metric Calibration Algorithm for Multifocus Plenoptic Cameras". In: *IEEE Transactions on Instrumentation and Measurement* 65.5, pp. 1197–1205.
- Johannsen, Ole et al. (2013). "On the calibration of focused plenoptic cameras". In: *Lecture Notes in Computer Science (including subseries Lecture Notes in Artificial Intelligence and Lecture Notes in Bioinformatics)* 8200 LNCS, pp. 302–317.

- Labussière, Mathieu et al. (2020). "Blur Aware Calibration of Multi-Focus Plenoptic Camera". In: *Proceedings of the IEEE/CVF Conference on Computer Vision and Pattern Recognition (CVPR)*, pp. 2545–2554.
- Ng, Ren et al. (2005). *Light Field Photography with a Hand-held Plenoptic Camera.* Tech. rep. Stanford University, pp. 1–11.
- Noury, Charles Antoine, Céline Teulière, and Michel Dhome (2017). "Light-Field Camera Calibration from Raw Images". In: *DICTA 2017 – International Conference on Digital Image Computing: Techniques and Applications*, pp. 1–8.
- Nousias, Sotiris et al. (2017). "Corner-Based Geometric Calibration of Multi-focus Plenoptic Cameras". In: *Proceedings of the IEEE International Conference on Computer Vision*, pp. 957–965.
- O'Brien, Sean et al. (2018). "Calibrating light-field cameras using plenoptic disc features". In: *2018 International Conference on 3D Vision (3DV)*. IEEE, pp. 286–294.

# References iv


- Pentland, Alex Paul (1987). "A New Sense for Depth of Field". In: *IEEE Transactions on Pattern Analysis and Machine Intelligence* PAMI-9.4, pp. 523–531.
- Perwaß, Christian and Lennart Wietzke (2012). "Single Lens 3D-Camera with Extended Depth-of-Field". In: *Human Vision and Electronic Imaging XVII*. Vol. 49. 431. SPIE, p. 829108.
- Shi, Shengxian et al. (2019). "Volumetric calibration enhancements for single-camera light-field PIV". In: *Experiments in Fluids* 60.1, p. 21.
- Subbarao, Murali (1989). *Determining Distance from Defocused Images of Simple Objects*. Tech. rep., pp. 11794–12350.
- Sun, Jun et al. (2016). "Geometric calibration of focused light field camera for 3-D flame temperature measurement". In: *Conference Record - IEEE Instrumentation and Measurement Technology Conference*.
- Wang, Yuan et al. (2018). "Virtual Image Points Based Geometrical Parameters' Calibration for Focused Light Field Camera". In: *IEEE Access* 6.c, pp. 71317–71326.

# References v


Zeller, Niclas et al. (2016). "Metric Calibration of a Focused Plenoptic Camera based on a 3D Calibration Target". In: *ISPRS Annals of Photogrammetry, Remote Sensing and Spatial Information Sciences* III-3.July, pp. 449–456.

Zhang, Chunping, Zhe Ji, and Qing Wang (2016). "Decoding and calibration method on focused plenoptic camera". In: *Computational Visual Media* 2.1, pp. 57–69.

Zhou, Ping et al. (2019). "A two-step calibration method of lenslet-based light field cameras". In: *Optics and Lasers in Engineering* 115, pp. 190–196.